Macroporous and Monolithic Anode Based on Polyaniline Hybridized Three-Dimensional Graphene for High-Performance Microbial Fuel Cells

Yang-Chun Yong,[†,§,¶] Xiao-Chen Dong,[‡,¶] Mary B. Chan-Park,[†] Hao Song,[†,⊥,*] and Peng Chen[†,*]

[†]School of Chemical and Biomedical Engineering, Nanyang Technological University, 70 Nanyang Drive, Singapore 637457, [‡]Key Laboratory for Organic Electronics & Information Displays (KLOEID) and Institute of Advanced Materials (IAM), Nanjing University of Posts and Telecommunications (NUPT), Nanjing, China 210046, [§]State Key Laboratory of Agricultural Microbiology, Hua Zhong Agricultural University, Wuhan, China 430070, and [⊥]Singapore Centre on Environmental Life Sciences Engineering (SCELSE), Nanyang Technological University, 60 Nanyang Drive, SBS-01n-27, Singapore 637551. [¶]These authors contributed equally to this work.

ABSTRACT Microbial fuel cell (MFC) is of great interest as a promising green energy source to harvest electricity from various organic matters. However, low bacterial loading capacity and low extracellular electron transfer efficiency between the bacteria and the anode often limit the practical applications of MFC. In this work, a macroporous and monolithic MFC anode based on polyaniline hybridized three-dimensional (3D) graphene is demonstrated. It outperforms the planar carbon electrode because of its abilities to three-dimensionally interface with bacterial biofilm, facilitate electron transfer, and provide multiplexed and highly conductive pathways. This study adds a new dimension to the MFC anode design as well as to the emerging graphene applications.

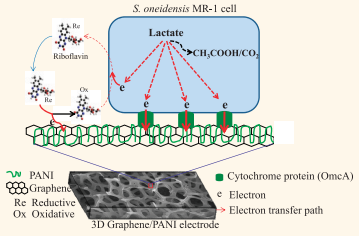

KEYWORDS: graphene · microbial fuel cell · green energy · nanotechnology

Microbial fuel cells (MFC) are sustainable and green energy sources that can convert chemical energy in organic wastes into electricity and integrate environmental bioremediation with power production.[1−3] Electrons stored in organic matters can be released by microbial metabolism and subsequently passed to solid electrodes in MFCs through different extracellular electron transfer (EET) mechanisms including direct electron transfer *via* the redox active proteins on the bacterial outer membrane and/or through the conductive pili (bacterial nanowires), and indirect electron transfer mediated by shuttle molecules.[3−5] However, the low output power density from MFCs due to low bacteria loading onto the electrode and low EET efficiency between bacteria and electrodes is the major bottleneck that obstructs practical applications of MFCs.[1,2]

Development of novel anodic materials that could facilitate bacterial biofilm formation and EET is vital to enhance power production of MFCs. Toward this aim, various strategies have been developed to increase the specific surface area, biocompatibility, conductivity, and electron-accepting ability of the electrodes.[6−10] For example, conducting nanostructured materials (*e.g.*, carbon nanotubes) have been employed to coat the standard electrode in order to increase the specific surface area and promote EET.[10] However, such flat (two-dimensional) porous anodes have small pore sizes. Consequently, bacteria only clog on the surface and are inaccessible to the interior of the anode. This seriously limits the anode efficiency. In view of this, three-dimensionally structured anodes have been devised based on graphite fiber brush,[11] reticulated vitreous carbon,[12] granular activated carbon,[13] carbon fiber nonwovens,[14] or carbon nanotube textile.[15] Compared with the conventional flat anodes, the three-dimensional (3D) anodes provide larger surface area to interface with bacteria. But the problems associated with these 3D structures include low specific surface area due to the lack of microscopic or nanoscopic structures, or too small pore sizes for bacteria penetration, or poor conductivity, or disruption of bacterial membrane by sharp nanomaterials.[16]

Graphene is a single atomic layer of carbon atoms arranged in a hexagonal lattice. Owing to its extraordinary electrical, physiochemical, and structural properties, this recently discovered allotrope of carbon has

* Address correspondence to songhao@ntu.edu.sg, chenpeng@ntu.edu.sg.

Received for review November 30, 2011 and accepted February 23, 2012.

Published online February 23, 2012
10.1021/nn204656d

already demonstrated great potentials in many fields of science and technologies.[17−27] It shall provide new opportunities to MFC as well, taking advantage of its unique properties, such as, outstanding electrical conductivity, extremely high specific surface area (up to ~2600 m^2/g), mechanical robustness and flexibility, chemical inertness, and biocompatibility.[28] Recently, thin-films of chemically derived graphene sheets[29] and graphene oxide nanoribbons[30] have been employed to improve the performance of MFC anodes. But the conductivity of those graphene materials is largely compromised by the chemical groups and defects introduced during the synthesis processes.[20,31] In addition, like other 2D structures, graphene thin-films have limited bacteria loading capacity and the stacking between individual sheets largely sacrifices the high intrinsic specific area of graphene. Herein, we demonstrate a novel 3D macroporous anode, which is a free-standing, flexible, conductive, and monolithic graphene foam[32] decorated with the conductive polymer polyaniline (PANI). To the best of our knowledge, this is the first demonstrated 3D monolithic carbon anode for MFC. We show that it greatly outperforms the standard planar carbon electrode owing to its abilities to three-dimensionally interface with bacterial biofilm, facilitate electron transfer, and provide multiplexed and highly conductive pathways.

RESULTS AND DISCUSSION

The 3D graphene was synthesized by chemical vapor deposition (CVD) with nickel foam as the substrate and using ethanol as the carbon source.[34] The nickel substrate was then etched away using a HCl (3M) solution at 80 °C to produce free-standing yet light graphene foam. As shown in Figure 1a, the 3D graphene exhibits a honeycomb structure with the pore size of 100−300 μm. At a higher magnification, it is observed that the surface of the graphene skeleton is seamlessly continuous and exhibits micrometer-scale smooth (flat) topographic domains (comparable to the size of a bacterium) (Figure 1b). The morphology, surface topology, and dimensions of 3D graphene are identical to those of the nickel substrate resulting from the conformal CVD growth. Therefore, these structural parameters of the 3D graphene can be varied by the choice of different growth substrates. Raman spectroscopy was also conducted to examine the obtained graphene (Figure 1c). The absence of Raman D band indicates that the grown graphene is of high quality, while the integrated intensity ratio between 2D and G band indicates the coexistence of single-layer and few-layer domains.[35,36] The lack of defects and absence of contacts between separated graphene sheets ensure a high conductivity of this 3D graphene monolith.

Despite that the graphene layers are extremely thin (one-atom thick for single-layer), the monolithically and continuously networked graphene structure can stand alone and be manipulated due to the extraordinary mechanical strength of graphene. As the 3D graphene foam gives a high specific surface area (~850 m^2/g),[32,33] it is able to provide a large surface area for bacteria attachment. Also desirably, the porosity of the graphene foam is much higher than that of carbon cloth (~99% *vs* ~65%).[15,32] Because the pore size of graphene foam is much larger than a bacterium (1−2 μm), bacteria can easily diffuse in and colonize inside. In addition, such macroporous structure guarantees unhindered substrate transport.

Graphene, however, just like other carbon materials is highly hydrophobic which is unfavorable for bacteria adhesion. We thus decorated the surface of graphene with hydrophilic conducting polymer PANI[6] through *in situ* polymerization in order to promote bacteria adhesion and biofilm formation. The success of PANI deposition was confirmed by scanning electron microscopy (SEM) (Figure 1d) and cyclic voltammetry (CV) (Figure 1e) in which the characteristic redox peaks from PANI (originated from the redox transition between the leucoemeraldine and the polaronicemeraldine form) are evident.

The performance of the 3D graphene/PANI anode was evaluated in comparison with that of carbon cloth (acommonly used anode material in MFCs). *Shewanella oneidensis* MR-1, a dissimilatory metal reducing bacterium, was selected here as the model electrogen[5] and lactate was used as the electron donor. As observed under SEM (Figure 2a,b), bacteria formed confluent biofilm on the PANI coated graphene surface. The SEM image of the electrode interior (Figure 2c) shows that the bacteria also densely adhere on the graphene surface deep inside the 3D electrode. This observation suggests that the macroporous structure of this 3D electrode allows sufficient substrate exchange to support internal bacterial biofilm growth, and implies that the biofilm loading on the electrode could be further improved by simply increasing the electrode thickness (1 mm thick graphene foam was used here). In comparison, bacterial bioflim formed only on some areas of the outmost surface of the bare 3D graphene and bacteria were not able at all to penetrate inside the 3D structure (Figure S1a and S1b in Supporting Information), indicating the critical role of PANI in recruiting bacteria onto the electrode. Not surprisingly, MFC equipped with bare 3D graphene anode gives poor electrical output (Figure S1c). Because PANI is positively charged in neutral solutions, it can electrostatically interact with the negatively charged bacterial membrane.[6] Carbon cloth is woven carbon microfibers (Figure 2d). After the commonly used acid treatment to render it hydrophilic, bacteria can densely adhere on carbon fibers on the surface of the carbon cloth (Figure 2e). But no bacteria can be found in the electrode interior (Figure 2f). The high 3D bacterial

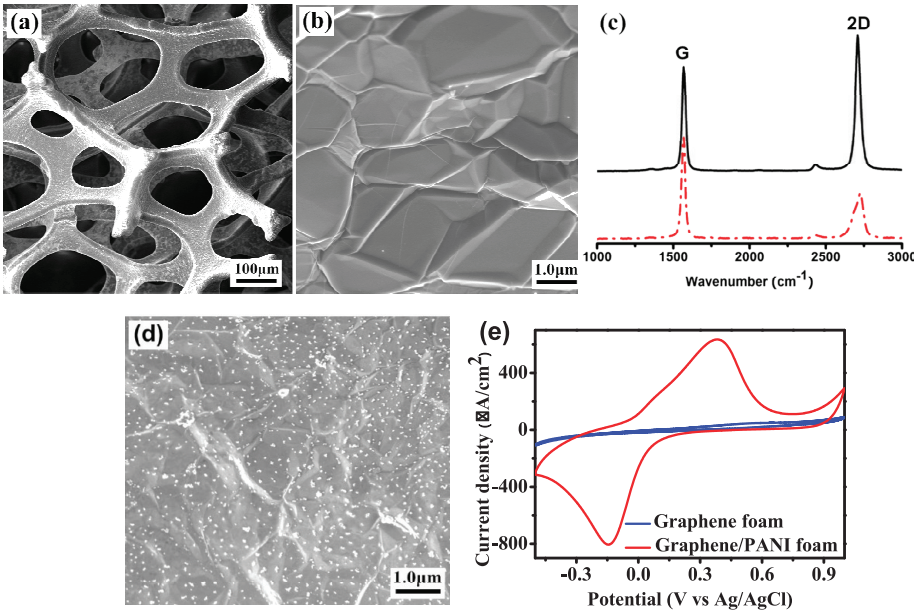

Figure 1. (a) SEM image of 3D graphene foam at low magnification. (b) SEM image at the graphene film at high magnification. (c) Raman spectra of graphene foams with different layers (solid line, single layer; dotted line, multilayer). (d) SEM image of PANI-modified graphene foam. (e) Cyclic voltammetry (CV) of the bare graphene foam electrode and the graphene/PANI foam electrode in PBS buffer (pH 7.2) at scan rate of 100 mV/s, respectively.

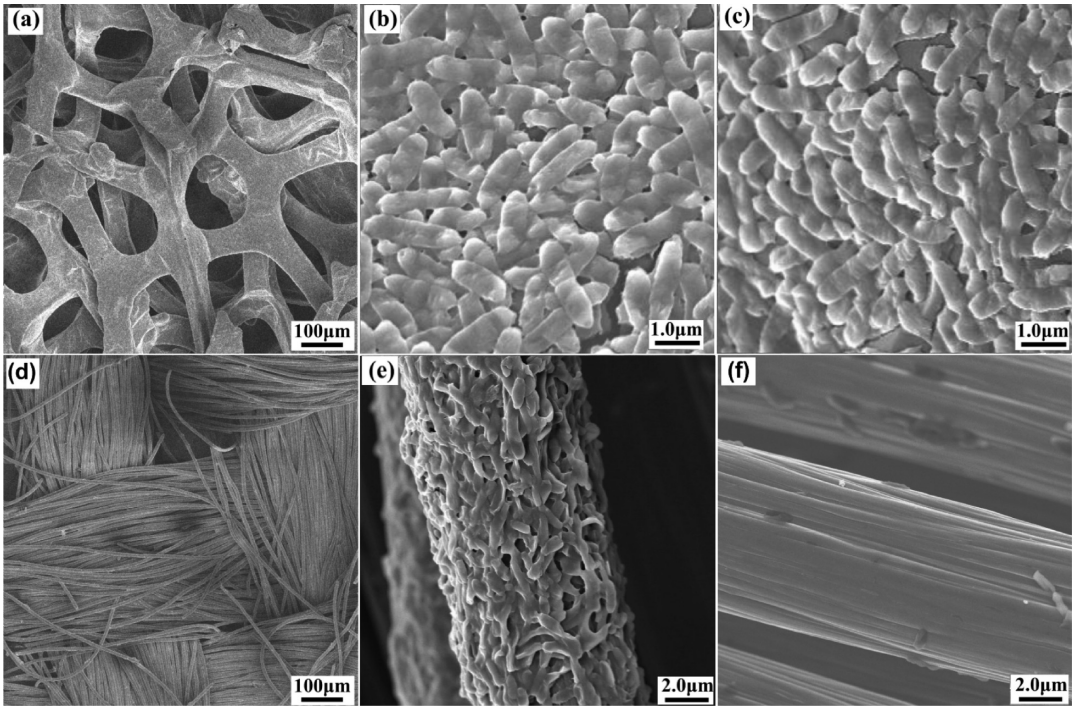

Figure 2. SEM images of graphene/PANI (a–c) and carbon cloth (d–f) electrodes after 60 h incubation in MFC with *S. oneidensis* MR-1 cell suspension. With a higher magnification, images b and e were taken at the electrode surface while images c and f were focused on the electrode interior.

loading capacity of our graphene/PANI anode is expected to guarantee a larger power output in MFC than that being afforded by a planar carbon cloth electrode.

S. oneidensis MR-1 has two distinct EET pathways, indirect transfer mediated by electron shuttles (riboflavin molecules) and direct electron transfer *via* c-type cytochromes proteins on its outer membrane.[5,37,38] As determined by high performance liquid chromatography (HPLC),[39] the concentrations of riboflavin released by the bacteria in the MFCs equipped with either a carbon cloth anode or 3D graphene/PANI anode did not show any difference (data not shown). However, the indirect electron transfer is presumably enhanced in the conductive 3D graphene, which provides a larger active

surface area to collect electrons from riboflavin molecules in solution. In addition, it has been demonstrated that PANI polymers can serve as conductive nanowires to enhance the extracellular electron transfer between bacteria and electrode through intimate contact with the redox active proteins on bacterial membrane.[6,40] Such direct electron transfer from the c-type cytochromes on the membrane *S. oneidensis* MR-1 to the 3D graphene/PANI electrode was indeed observed in our cyclic voltammogram (CV) analysis, whereas it was absent in the carbon cloth electrode (Figure 3a).

The CV plot of the carbon cloth anode shows a pair of redox peaks (Figure 3a), which are believed to originate from some unidentified bacterial metabolites.[41] They are not related to the electron transfer from the bacteria because the midpoint potential of these redox peaks (~0.3 V) is very close to the cathode potential (~0.3 V) and much higher than the reaction potential of our MFC anode (<0 V). The CV of the graphene/PANI foam exhibits several characteristic redox peaks that are missing from that of the carbon cloth (Figure 3a). First, the two peaks denoted as a and b result from the redox transition of PANI. These two large peaks mask the weaker redox peaks observed in the carbon cloth. In addition to these, two more redox peaks are identified: a cathodic peak c at *ca.* −0.38 V and a rather weak and broad anodic peak d. The peak d can be more clearly observed in the semiderivative plot (inset of Figure 3a and Supporting Information, Figure S2a), which is a technique commonly used to differentiate peaks from complex CV plots.[42] The peaks c and d coincide, in terms of voltage positions and amplitudes, with the asymmetric redox peaks produced by the outer-membrane c-type cytochrome proteins (MtrC or OmcA) of *S. oneidensis* MR-1 that are responsible for the direct electron transfer between the bacterium and the electrode.[10,43,44] The midpoint potential of this redox pairs was estimated to be *ca.* −0.265 V (Supporting Information, Figure S2a), which is in good accordance with that of OmcA.[10] Moreover, similar to the observation made with OmcA, the magnitudes of these redox peaks (c and d) reduced and the position of reductive peak (c) shifted positively in the second CV scan (Supporting Information, Figure S2b). Taken together, it can be concluded that the garphene/PANI foam is able to harvest electrons *via* direct electron transfer from OmcA cytochrome proteins on *S. oneidensis* MR-1, whereas the carbon cloth anode is incapable of it.

Electrochemical impedance spectroscopy (EIS) analysis[7] was then carried out to investigate the charge-transfer resistance of the MFCs equipped with the carbon cloth anode or the 3D graphene/PANI foam anode (Figure 3b). The EIS Nyquist plot is the superimposition of a preceding frequency-dependent semicircle (high frequency region) and a following straight line (low frequency region); the diameter of the former

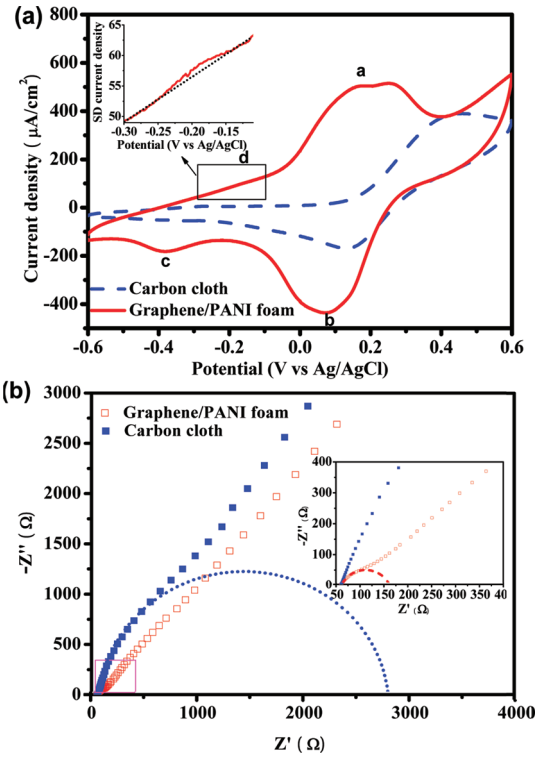

Figure 3. Electrochemical characterizations of carbon cloth anode and graphene/PANI anode in MFC. (a) The cyclic voltammetry (CV) of the carbon cloth anode and the graphene/PANI anode in the MFC, at the scan rate of 30 mV/s. The inset shows the semiderivative (SD) CV of the selected voltage range where the dashed line indicates the baseline. (b) Nyquist plots of the two types of anodes in MFCs (0.01 Hz to 100 kHz for graphene/PANI foam; 0.04 Hz to 100 kHz for carbon cloth; at open-circuit potential and with a perturbation signal of 10 mV). The inset depicts the enlarged view of the indicated square region. The dashed semicircles are drawn based on fitting.

indicates the charge-transfer resistance.[7,45] As shown in Figure 3b, the charge-transfer resistance of graphene/PANI MFC (~100 Ω) is much smaller than that of carbon cloth MFC (~2800 Ω). A smaller charge-transfer resistance is resulted from a faster electron transfer rate.[7] This confirms that the EET efficiency of 3D graphene/PANI is much higher than that of carbon cloth.

Higher bacterial loading and higher EET efficiency of the 3D graphene/PANI anode enable its higher output power density than the carbon cloth anode. To verify this, the performance of the two types of anodes was tested in parallel in two-chamber MFCs (with a load resistance of 2 kΩ). As shown in Figure 4a, the power density of the MFC equipped with a carbon cloth anode reached its plateau at 6 h with a power density of ~110 mW/m^2. The power density of the MFC equipped with a 3D graphene/PANI foam reached the similar level at 6 h, and then increased further to a plateau (~190 mW/m^2) at about 24 h. The plateau power density of the 3D graphene/PANI MFCs is significantly higher than that of the carbon cloth MFCs (88.7 ± 10.9% higher, n = 4). However, such

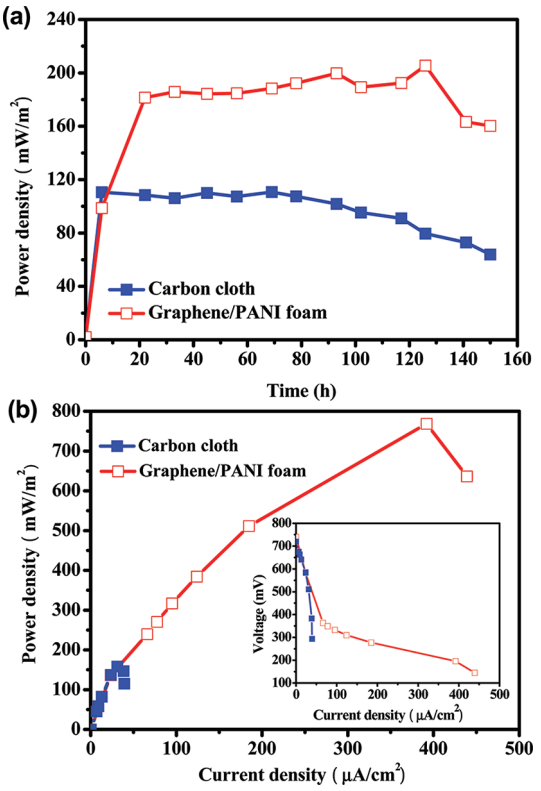

Figure 4. (a) Time courses of the power density output of the MFCs equipped with a carbon cloth anode or a graphene/PANI foam anode. (b) Polarization curves of the two types of MFCs. The inset shows the *I*–*V* relation.

improvement is still underestimated because of the huge mismatch between the internal resistance of 3D graphene/PANI MFCs and the loading resistance. The maximally attainable power achieved at the perfect match between the internal resistance and the load resistance can be determined using the polarization curve.[7] As shown in Figure 4b, the maximum power density obtained from the 3D graphene/PANI MFC is ~768 mW/m^2, which is about 4 times higher than that from the carbon cloth MFC (~158 mW/m^2). Furthermore, since graphene/PANI foam is much lighter than carbon cloth (3 g/m^2 *vs* 136 g/m^2), it produces about 212 times higher specific power density than carbon cloth (256 mW/g *vs* 1.2 mW/g). Thus, the 3D graphene/PANI electrode is advantageous for use as high-power large-scale MFCs.

The 3D graphene/PANI electrode also significantly outperforms the PANI-coated carbon cloth electrode and carbon felt electrode with or without PANI coating (Table 1). These experiments demonstrate the advantage of the 3D carbon electrode over the 2D carbon electrodes. Noteworthy, the redox waves from the c-type cytochromes were not observed in the CV analysis of the MFCs equipped with a bare 3D graphene or carbon cloth/PANI anode (Supporting Information, Figure S3). The results suggest that the synergistic integration between 3D graphene and

TABLE 1. Maximum Power Density Output Obtained from Different Anode Materials

electrode	power density (mW/m^2)	specific power density (mW/g)
carbon cloth (CC)	158	1.16
CC/PANI	323	2.37
carbon felt (CF)	10.8	0.09
CF/PANI	145	1.20
nickel foam	21.9	0.05
nickel foam/PANI	70.8	0.17
graphene foam	12.8	4.26
graphene/PANI foam	768	256

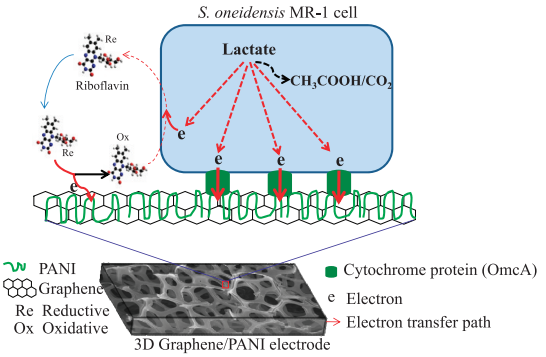

Figure 5. Schematic illustration of the interface between 3D graphene/PANI monolith electrode and *S. oneidensis* MR-1 bacteria.

PANI is the key to promoting direct electron transfer between bacteria and electrode. To illustrate the critical benefits of graphene, we used nickel foam as a 3D metallic electrode for comparison. It was found that the nickle foam anodes with or without PANI coating give poor performance (Table 1). Carbon fiber brush is regarded as a 3D carbon anode for MFCs. It is worth pointing out that the power density output of our MFC with the 3D graphene/PANI anode is much higher than that from a previously reported MFC using a carbon fiber brush anode and the same bacterial strain as ours (768 *vs* 332 mW/m^2).[46] Furthermore, as summarized in Table S1 (Supporting Information), the performance of our MFC is clearly superior to the previously reported MFCs which used the same bacterial strain, similar experimental setup, yet different anodes.

CONCLUSION

In summary, we demonstrate the use of a novel 3D graphene/PANI structure as the MFC anode. It impressively outperforms the commonly used carbon cloth owing to the higher bacterial biofilm loading and higher EET efficiency (Figure 5). The former is due to the large specific surface area of the 3D graphene/PANI electrode and its ability to integrate with bacterial biofilms three-dimensionally. The latter is because of the large surface area to accept electrons from riboflavin molecules (electron shuttles released by

S. oneidensis MR-1), realization of direct electron transfer from OmcA cytochrome proteins on cell membrane, and the multiplexing and highly conductive pathways provided by the graphene network. In addition, this 3D anode is promising for practical large-scale MFCs because its lightness ensures high specific power density and its power output can be boosted simply by increasing its thickness. Furthermore, because the 3D graphene electrode is monolithic (continuous scaffold as a whole) and with smooth surface, the bacterial membrane will not be disrupted due to penetration of sharp nanoscale features, and cytotoxicity will not arise due to uptake of nanomaterials. This study adds a new dimension to MFC anode design as well as to the emerging graphene applications.

METHODS

Preparation and Characterizations of 3D Graphene Foams. The nickel foam substrates (1 mm thick) were cut into 1 cm × 1 cm pieces, loaded into a quartz tube, and heated at 1000 °C under H_2 (25 sccm) and Ar (50 sccm) atmosphere for 10 min to clean the surface of nickel foam. Then, ethanol vapor as the carbon source was introduced into the tube by bubbling H_2/Ar gas mixture through an ethanol liquid at ambient pressure. After 20 min of the chemical vapor deposition (CVD) growth process, the quartz tube was rapidly cooled down to room temperature at a rate of ~100 °C/min. Finally, the nickel substrates were etched away with HCl (3M) solution at 80 °C to obtain free-standing 3D graphene foam. Polyaniline (PANI) polymers were deposited on the surface of graphene foams or other electrodes by rapid-mixture polymerization of aniline monomers under acid condition with ammonium persulfate (APS) as the catalyst.[47,48] Specifically, 20 mL of 1 M HCl with 6.4 mmol aniline was rapidly mixed with another 20 mL 1 M HCl solution containing 1.6 mmol APS, with constant stirring to ensure homogeneous mixing. Then the 3D graphene foams or other electrodes fixed on a glass substrate were carefully immersed into the mixed solution. After 24 h reaction at room temperature, the 3D graphene foams were taken out, washed with DI water, and dried in an oven at 50 °C to obtain 3D graphene−PANI hybrids. The morphology and structure were characterized by field-emission scanning electron microscopy (JSM6700-FESEM, JEOL) and Raman spectroscopy (laser wavelength 488 nm) (CRM200 Confocal Raman, WITec).

Bacterial Culture. A 1.5 mL aliquot of *S. oneidensis* MR-1 bacterial culture suspension was inoculated in 150 mL of fresh LB broth[41] and incubated with shaking at 37 °C until the optical density at 600 nm (OD600) reached about 1.0. The cell pellets were then harvested by centrifugation (5000*g* × 5 min) and washed 3 times with M9 buffer.[41] Subsequently, the cell pellets were resuspended in 150 mL anaerobic electrolyte (5% LB broth plus 95% M9 buffer) supplemented with 18 mM lactate.[9] The cell suspension (~10^9 cells/mL) were transferred into the anodic chamber of the MFC and purged with nitrogen gas for 30 min to remove the dissolved oxygen. Finally, the anodic chamber was tightly sealed to maintain the anaerobic condition during MFC operation.

MFC Setup and Electrochemcial Measurement. A dual chamber MFC (5.5 cm × 5.5 cm × 6 cm) separated with nafion 117 membrane was used in this work.[41] Carbon cloth (2 cm × 4 cm) was used as the cathode electrode. Carbon cloth, carbon cloth/PANI, carbon felt, carbon felt/PANI, nickel foam, nickel foam/PANI, graphene foam, and graphene/PANI foam (1 cm × 1 cm for all) were used as the anodic electrodes. The anodic chamber contained *S. oneidensis* MR-1 cell suspension, and the cathodic chamber was filled with 50 mM $K_3[Fe(CN)_6]$ and KCl solution. At the steady-state of MFC, the polarization curves were obtained by varying the external resistor.[49] Current density (I) was calculated as $I = V$ (output voltage)/R (external resistance), and power density (P) was calculated as $P = V \times I$. Both I and P were normalized to the projected area of anode surface. The output voltage (V) across the external loading resistance (R) was measured by a digital multimeter (ESCORT 3146A). The electrochemical measurements (CV and EIS) were conducted using CHI 660D electrochemical working station (CH Instrument, Shanghai, China) with an Ag/AgCl−KCl saturated reference electrode.

Conflict of Interest: The authors declare no competing financial interest.

Acknowledgment. This work was supported by an AcRF tier 2 grant (Singapore, Grant MOE2011-T2-2-010), a CRP grant (Singapore, Grant NRF-CRP-07-2), SUG grant (Singapore), AcRF Tier-1 grant (Singapore, Grant RG78/10), the NNSF of China (Grants 50902071, 61076067 and BZ2010043), 973 Program (China, Grants 2009CB930601 and 2012CB933301), the Priority Academic Program Development of Jiangsu Higher Education Institutions, the Ministry of Education (China, Grant IRT1148).

Supporting Information Available: Additional information on MFC performance of bare 3D graphene, CV plots of OmcA, CV plots of carbon cloth/PANI anode, and the bare graphene foam anode, and performance comparison between our MFC with the reported in the literature. This material is available free of charge *via* the Internet at http://pubs.acs.org.

REFERENCES AND NOTES

1. Zhao, F.; Slade, R. C. T.; Varcoe, J. R. Techniques for the Study and Development of Microbial Fuel Cells: An Electrochemical Perspective. *Chem. Soc. Rev.* **2009**, *38*, 1926–1939.
2. Logan, B. E. Exoelectrogenic Bacteria that Power Microbial Fuel Cells. *Nat. Rev. Microbiol.* **2009**, *7*, 375–381.
3. Lovley, D. R. Bug Juice: Harvesting Electricity with Microorganisms. *Nat. Rev. Microbiol.* **2006**, *4*, 497–508.
4. Schroder, U. Anodic Electron Transfer Mechanisms in Microbial Fuel Cells and Their Energy Efficiency. *Phys. Chem. Chem. Phys.* **2007**, *9*, 2619–2629.
5. Jiang, X. C.; Hu, J. S.; Fitzgerald, L. A.; Biffinger, J. C.; Xie, P.; Ringeisen, B. R.; Lieber, C. M. Probing Electron Transfer Mechanisms in *Shewanella oneidensis* MR-1 Using a Nanoelectrode Platform and Single-Cell Imaging. *Proc. Natl. Acad. Sci. U.S.A.* **2010**, *107*, 16806–16810.
6. Lai, B.; Tang, X.; Li, H.; Du, Z.; Liu, X.; Zhang, Q. Power Production Enhancement with a Polyaniline Modified Anode in Microbial Fuel Cells. *Biosens. Bioelectron.* **2011**, *28*, 373–377.
7. Qiao, Y.; Bao, S. J.; Li, C. M.; Cui, X. Q.; Lu, Z. S.; Guo, J. Nanostructured Polyaniline/Titanium Dioxide Composite Anode for Microbial Fuel Cells. *ACS Nano* **2008**, *2*, 113–119.
8. Liu, C. J.; Burghaus, U.; Besenbacher, F.; Wang, Z. L. Preparation and Characterization of Nanomaterials for Sustainable Energy Production. *ACS Nano* **2010**, *4*, 5517–5526.
9. Yu, Y. Y.; Chen, H. L.; Yong, Y. C.; Kim, D. H.; Song, H. Conductive Artificial Biofilm Dramatically Enhances Bioelectricity Production in *Shewanella*-Inoculated Microbial Fuel Cells. *Chem. Commun.* **2011**, *47*, 2825–2827.
10. Peng, L.; You, S. J.; Wang, J. Y. Carbon Nanotubes as Electrode Modifier Promoting Direct Electron Transfer from *Shewanella oneidensis*. *Biosen. Bioelectron.* **2010**, *25*, 1248–1251.
11. Logan, B.; Cheng, S.; Watson, V.; Estadt, G. Graphite Fiber Brush Anodes for Increased Power Production in

Air−Cathode Microbial Fuel Cells. *Environ. Sci. Technol.* **2007**, *41*, 3341–3346.
12. He, Z.; Minteer, S. D.; Angenent, L. T. Electricity Generation from Artificial Wastewater Using an Upflow Microbial Fuel Cell. *Environ. Sci. Technol.* **2005**, *39*, 5262–5267.
13. He, Z.; Wagner, N.; Minteer, S. D.; Angenent, L. T. An Upflow Microbial Fuel Cell with an Interior Cathode: Assessment of the Internal Resistance by Impedance Spectroscopy. *Environ. Sci. Technol.* **2006**, *40*, 5212–5217.
14. Chen, S. L.; Hou, H. Q.; Harnisch, F.; Patil, S. A.; Carmona-Martinez, A. A.; Agarwal, S.; Zhang, Y. Y.; Sinha-Ray, S.; Yarin, A. L.; Greiner, A.; *et al.* Electrospun and Solution Blown Three-Dimensional Carbon Fiber Nonwovens for Application as Electrodes in Microbial Fuel Cells. *Energy Environ. Sci.* **2011**, *4*, 1417–1421.
15. Xie, X.; Hu, L.; Pasta, M.; Wells, G. F.; Kong, D.; Criddle, C. S.; Cui, Y. Three-Dimensional Carbon Nanotube-Textile Anode for High-Performance Microbial Fuel Cells. *Nano Lett.* **2011**, *11*, 291–296.
16. Kang, S.; Pinault, M.; Pfefferle, L. D.; Elimelech, M. Single-Walled Carbon Nanotubes Exhibit Strong Antimicrobial Activity. *Langmuir* **2007**, *23*, 8670–8673.
17. Huang, Y.; Dong, X.; Shi, Y.; Li, C. M.; Li, L. J.; Chen, P. Nanoelectronic Biosensors Based on CVD Grown Graphene. *Nanoscale* **2010**, *2*, 1485–1488.
18. Hou, J. B.; Shao, Y. Y.; Ellis, M. W.; Moore, R. B.; Yi, B. L. Graphene-Based Electrochemical Energy Conversion and Storage: Fuel Cells, Supercapacitors and Lithium Ion Batteries. *Phys. Chem. Chem. Phys.* **2011**, *13*, 15384–15402.
19. Sudibya, H. G.; He, Q. Y.; Zhang, H.; Chen, P. Electrical Detection of Metal Ions Using Field-Effect Transistors Based on Micropatterned Reduced Graphene Oxide Films. *ACS Nano* **2011**, *5*, 1990–1994.
20. Guo, S.; Dong, S. Graphene Nanosheet: Synthesis, Molecular Engineering, Thin Film, Hybrids, and Energy and Analytical Applications. *Chem. Soc. Rev.* **2012**, *40*, 2644–72.
21. Freitag, M. Graphene—Nanoelectronics Goes Flat Out. *Nat. Nanotechnol.* **2008**, *3*, 455–457.
22. Liu, Y.; Dong, X.; Chen, P. Biological and Chemical Sensors Based on Graphene Materials. *Chem. Soc. Rev.* **2012**, *41*, 2283−2307.
23. Wang, S. Y.; Yu, D. S.; Dai, L. M.; Chang, D. W.; Baek, J. B. Polyelectrolyte-Functionalized Graphene as Metal-Free Electrocatalysts for Oxygen Reduction. *ACS Nano* **2011**, *5*, 6202–6209.
24. Qu, L. T.; Liu, Y.; Baek, J. B.; Dai, L. M. Nitrogen-Doped Graphene as Efficient Metal-Free Electrocatalyst for Oxygen Reduction in Fuel Cells. *ACS Nano* **2010**, *4*, 1321–1326.
25. Choi, B. G.; Hong, J.; Park, Y. C.; Jung, D. H.; Hong, W. H.; Hammond, P. T.; Park, H. Innovative Polymer Nanocomposite Electrolytes: Nanoscale Manipulation of Ion Channels by Functionalized Graphenes. *ACS Nano* **2011**, *5*, 5167–5174.
26. Choi, B. G.; Hong, J.; Hong, W. H.; Hammond, P. T.; Park, H. Facilitated Ion Transport in All-Solid-State Flexible Supercapacitors. *ACS Nano* **2011**, *5*, 7205–7213.
27. Choi, B. G.; Park, H.; Park, T. J.; Yang, M. H.; Kim, J. S.; Jang, S. Y.; Heo, N. S.; Lee, S. Y.; Kong, J.; Hong, W. H. Solution Chemistry of Self-Assembled Graphene Nanohybrids for High-Performance Flexible Biosensors. *ACS Nano* **2010**, *4*, 2910–2918.
28. Agarwal, S.; Zhou, X.; Ye, F.; He, Q.; Chen, G. C.; Soo, J.; Boey, F.; Zhang, H.; Chen, P. Interfacing Live Cells with Nanocarbon Substrates. *Langmuir* **2010**, *26*, 2244–2247.
29. Zhang, Y. Z.; Mo, G. Q.; Li, X. W.; Zhang, W. D.; Zhang, J. Q.; Ye, J. S.; Huang, X. D.; Yu, C. Z. A Graphene Modified Anode to Improve the Performance of Microbial Fuel Cells. *J. Power Sources* **2011**, *196*, 5402–5407.
30. Huang, Y. X.; Liu, X. W.; Xie, J. F.; Sheng, G. P.; Wang, G. Y.; Zhang, Y. Y.; Xu, A. W.; Yu, H. Q. Graphene Oxide Nanoribbons Greatly Enhance Extracellular Electron Transfer in Bio-electrochemical Systems. *Chem. Commun.* **2011**, *47*, 5795–5797.
31. Dong, X. C.; Su, C. Y.; Zhang, W. J.; Zhao, J. W.; Ling, Q. D.; Huang, W.; Chen, P.; Li, L. J. Ultra-Large Single-Layer Graphene Obtained from Solution Chemical Reduction and its Electrical Properties. *Phys. Chem. Chem. Phys.* **2010**, *12*, 2164–2169.
32. Chen, Z.; Ren, W.; Gao, L.; Liu, B.; Pei, S.; Cheng, H. M. Three-Dimensional Flexible and Conductive Interconnected Graphene Networks Grown by Chemical Vapour Deposition. *Nat. Mater.* **2011**, *10*, 424–428.
33. Cao, X. H.; Shi, Y. M.; Shi, W. H.; Lu, G.; Huang, X.; Yan, Q. Y.; Zhang, Q. C.; Zhang, H. Preparation of Novel 3D Graphene Networks for Supercapacitor Applications. *Small* **2011**, *7*, 3163–3168.
34. Dong, X. C.; Wang, P.; Fang, W. J.; Su, C. Y.; Chen, Y. H.; Li, L. J.; Huang, W.; Chen, P. Growth of Large-Sized Graphene Thin-Films by Liquid Precursor-Based Chemical Vapor Deposition under Atmospheric Pressure. *Carbon* **2011**, *49*, 3672–3678.
35. Huang, Y. X.; Dong, X. C.; Liu, Y. X.; Li, L. J.; Chen, P. Graphene-Based Biosensors for Detection of Bacteria and Their Metabolic Activities. *J. Mater. Chem.* **2011**, *21*, 12358–12362.
36. Graf, D.; Molitor, F.; Ensslin, K.; Stampfer, C.; Jungen, A.; Hierold, C.; Wirtz, L. Spatially Resolved Raman Spectroscopy of Single- and Few-Layer Graphene. *Nano Lett.* **2007**, *7*, 238–242.
37. Coursolle, D.; Baron, D. B.; Bond, D. R.; Gralnick, J. A. The Mtr Respiratory Pathway Is Essential for Reducing Flavins and Electrodes in *Shewanella oneidensis*. *J. Bacteriol.* **2010**, *192*, 467–474.
38. Xiong, Y. J.; Shi, L.; Chen, B. W.; Mayer, M. U.; Lower, B. H.; Londer, Y.; Bose, S.; Hochella, M. F.; Fredrickson, J. K.; Squier, T. C. High-Affinity Binding and Direct Electron Transfer to Solid Metals by the *Shewanella oneidensis* MR-1 Outer Membrane c-Type Cytochrome OmcA. *J. Am. Chem. Soc.* **2006**, *128*, 13978–13979.
39. Peng, L.; You, S. J.; Wang, J. Y. Electrode Potential Regulates Cytochrome Accumulation on *Shewanella oneidensis* Cell Surface and the Consequence to Bioelectrocatalytic Current Generation. *Biosens. Bioelectron.* **2010**, *25*, 2530–2533.
40. Zhao, Y.; Watanabe, K.; Nakamura, R.; Mori, S.; Liu, H.; Ishii, K.; Hashimoto, K. Three-Dimensional Conductive Nanowire Networks for Maximizing Anode Performance in Microbial Fuel Cells. *Chem.—Eur. J.* **2010**, *16*, 4982–4985.
41. Yong, Y. C.; Yu, Y. Y.; Li, C. M.; Zhong, J. J.; Song, H. Bioelectricity Enhancement *via* Overexpression of Quorum Sensing System in *Pseudomonas aeruginosa*-Inoculated Microbial Fuel Cells. *Biosens. Bioelectron.* **2011**, *30*, 87–92.
42. Palys, M.; Korba, T.; Bos, M.; Vanderlinden, W. E. The Separation of Overlapping Peaks in Cyclic Voltammetry by Means of Semi-differential Transformation. *Talanta* **1991**, *38*, 723–733.
43. Eggleston, C. M.; Voros, J.; Shi, L.; Lower, B. H.; Droubay, T. C.; Colberg, P. J. S. Binding and Direct Electrochemistry of OmcA, an Outer-Membrane Cytochrome from an Iron Reducing Bacterium, with Oxide Electrodes: A Candidate Biofuel Cell System. *Inorg. Chim. Acta* **2008**, *361*, 769–777.
44. Meitl, L. A.; Eggleston, C. M.; Colberg, P. J. S.; Khare, N.; Reardon, C. L.; Shi, L. Electrochemical Interaction of *Shewanella oneidensis* MR-1 and Its Outer Membrane Cytochromes OmcA and MtrC with Hematite Electrodes. *Geochim. Cosmochim. Acta* **2009**, *73*, 5292–5307.
45. He, Z.; Mansfeld, F. Exploring the Use of Electrochemical Impedance Spectroscopy (EIS) in Microbial Fuel Cell Studies. *Energy Environ. Sci.* **2009**, *2*, 215–219.
46. Watson, V. J.; Logan, B. E. Power Production in MFCs Inoculated with *Shewanella oneidensis* MR-1 or Mixed Cultures. *Biotechnol. Bioeng.* **2010**, *105*, 489–498.
47. Yan, X. B.; Chen, J. T.; Yang, J.; Xue, Q. J.; Miele, P. Fabrication of Free-Standing, Electrochemically Active, and Biocompatible Graphene Oxide−Polyaniline and Graphene−Polyaniline Hybrid Papers. *ACS Appl. Mater. Inter.* **2010**, *2*, 2521–2529.
48. Wu, Q.; Xu, Y.; Yao, Z.; Liu, A.; Shi, G. Supercapacitors Based on Flexible Graphene/Polyaniline Nanofiber Composite Films. *ACS Nano* **2010**, *4*, 1963–1970.
49. Logan, B. E.; Hamelers, B.; Rozendal, R. A.; Schrorder, U.; Keller, J.; Freguia, S.; Aelterman, P.; Verstraete, W.; Rabaey, K. Microbial Fuel Cells: Methodology and Technology. *Environ. Sci. Technol.* **2006**, *40*, 5181–5192.